Membrane Mechanics Can Account for Fusion Pore Dilation in Stages

Y. A. Chizmadzhev,* F. S. Cohen,‡ A. Shcherbakov,* and J. Zimmerberg§
*Frumkin Institute of Electrochemistry, Moscow, Russia; ‡Rush Medical College, Department of Physiology, Chicago, Illinois 60612 USA; and §Laboratory of Theoretical and Physical Biology, National Institute of Child Health and Human Development, National Institutes of Health, Bethesda, Maryland 20892 USA

ABSTRACT Once formed, fusion pores rapidly enlarge to semi-stable conductance values. The membranes lining the fusion pore are continuous bilayer structures, so variations of conductance in time reflect bending and stretching of membranes. We therefore modeled the evolution of fusion pores using the theory of the mechanics of deforming homogeneous membranes. We calculated the changes in length and width of theoretical fusion pores according to standard dynamical equations of motion. Theoretical fusion pores quickly achieve semi-stable dimensions, which correspond to energy minima located in a canyon between energy barriers. The height of the barrier preventing pore expansion diminishes along the dimensions of length and width. The bottom of the canyon slopes gently downward along increasing length. As a consequence, theoretical fusion pores slowly lengthen and widen as the dimensions migrate along the bottom of the canyon, until the barrier vanishes and the pore rapidly enlarges. The dynamics of growth is sensitive to tension, spontaneous curvature, bending elasticity, and mobilities. This sensitivity can account for the quantitative differences in pore evolution observed in two experimental systems: HA-expressing cells fusing to planar bilayer membranes and beige mouse mast cell degranulation. We conclude that the mechanics of membranes could cause the phenomenon of stagewise growth of fusion pores.

INTRODUCTION

Fusion pores are the structures that connect fusing membranes and allow mixing of aqueous contents (White, 1992). The initial pore is small, both in exocytotic secretion from mast cells (Zimmerberg et al., 1987; Breckenridge and Almers, 1987; Spruce et al., 1990; Nanavati et al., 1992; Curran et al., 1993) and in fusion of HA-expressing cells to erythrocytes (Spruce et al., 1989, 1991; Tse et al., 1993; Zimmerberg et al., 1994) or to planar membranes (Melikyan et al., 1993a,b). For both mast cell exocytosis (Curran et al., 1993) and fusion of HA-expressing cells to planar membranes (Melikyan et al., 1993b), fusion pores grow in stages. The small initial pores rapidly grow to conductances that vary within restricted ranges for extended times. Within this semi-stable (S) stage, the pore conductance fluctuates, with the mean conductance remaining constant or monotonically increasing. Pores then grow to even larger conductances. Although the exocytotic and cell-bilayer systems share the motif of pore growth in stages, they exhibit quantitative differences. These can be seen from Fig. 1, where pore growth is shown for the two systems. The semi-stable stage typically lasts for a few milliseconds to a second for mast cell secretion (Fig. 1 *A*), but for tens of milliseconds to several seconds for cell-planar membrane fusion (Fig. 1 *B*). Furthermore, the fusion pore leaves this S stage with an immeasurably fast (<1 ms) characteristic rise time for the cell-bilayer system, whereas the rise time is usually significantly slower for cellular secretion.

For pores to grow, the membranes of the pore must be bent, stretched, and otherwise deformed. We therefore theoretically modeled pore evolution assuming that the mechanics of membrane deformation alone controlled pore growth. The mechanics of phospholipid membranes have been extensively studied both experimentally and theoretically (Evans and Skalak, 1980; Meunier et al., 1987). A model for the energy required to bend a membrane into a fusion pore (Kozlov et al., 1989) has been used to consider the enlargement of a pore with varying diameter but fixed length (Nanavati et al., 1992). We have extended this treatment and have allowed both the length and diameter of the pore to change according to standard dynamical equations of motion. When the mobilities of the length and diameter variables are different, membrane mechanics predicts pore growth in stages in two fusion systems: biological exocytosis and fusion of cells to planar phospholipid membranes. A report of some aspects of this paper has been published in Russian (Chizmadzhev et al., 1995).

FUSION PORE MODEL AND THEORETICAL APPROACHES

Pore model and energy

Freeze-fracture electron microscopy shows that fusion pores, for the most part, are hourglass shaped (Curran et al., 1993). We approximate the pore as a toroid (Fig. 2), smoothly connecting two membranes with an external radius R of the neutral surface of the toroid (surface of zero compression and expansion) and an inner radius r of the neutral surface at its narrowest portion. The wall of the pore is a complex structure. The two lipid monolayers, each with

Received for publication 30 December 1994 and in final form 8 September 1995.

Address reprint requests to Dr. Joshua Zimmerberg, National Insitutes of Health, Building 10, Room 10D14, 10 Center Drive, MSC 1855, Bethesda, MD 20892-1855. Tel.: 301-496-6571; Fax: 301-594-0813; E-mail: joshz@helix.nih.gov.

0006-3495/95/12/2489/12 $2.00

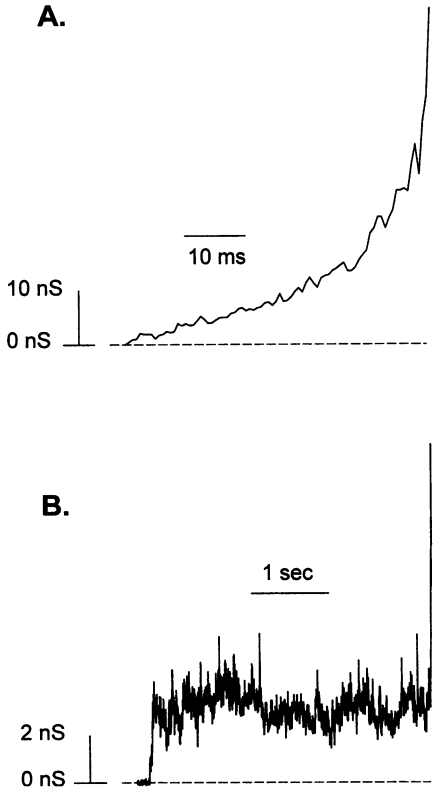

FIGURE 1 Fusion pore conductance grows in stages. (*A*) Exocytotic fusion pore of a beige mouse mast cell, exactly as in Curran et al. (1993). (*B*) Viral fusion pore of influenza HA-expressing (Hab2) cell fusing to a solvent-free planar phospholipid bilayer membrane made from dioleoylphosphatidylcholine/bovine brain phosphatidylethanolamine 2:1 (w/w) with 5 molar % of brain gangliosides G_{D1a}/G_{T1b} 1:1 (w/w) in squalene, exactly as in Melikyan et al. (1993b).

spontaneous curvatures (Siegel, 1993), can be coupled by membrane proteins that span the membrane and supramolecular structures that can in turn alter the spontaneous curvature of the entire membrane. We simplify by assuming that the wall of the fusion pore is mechanically homogeneous, with a bending modulus of elasticity B and a spontaneous curvature K_s. The two curvatures of the neutral surface, shown in cross section in Fig. 2, have opposite

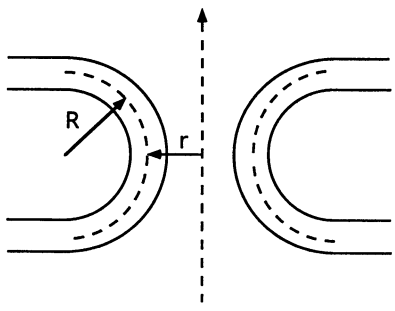

FIGURE 2 Geometrical model of the fusion pore. The pore is approximated as a toroid with external radius R of the neutral surface (*dashed line*). The inner radius r of the pore is the narrowest radius from the central axis of rotation to the neutral surface.

signs. The curvature corresponding to r is negative, whereas that corresponding to R is positive. Once formed, a fusion pore consists of bilayer membrane created from the two fusing membranes. The bending elastic energy, E_b, of the membrane is described as a quadratic function of the principal radii of curvatures, R_1 and R_2, of the neutral surface of the pore's membrane (Helfrich, 1973),

$$E_b = \frac{B}{2}\int\left(\frac{1}{R_1}+\frac{1}{R_2}-2K_s\right)^2 dS - 2BK_s^2\int dS,$$

where the integration is over the neutral surface. The bending elastic energy for a toroid is (Kozlov et al., 1989)

$$E_b = 2\pi B\left\{\frac{2(r+R)^2}{R\sqrt{r(r+2R)}}\arctan\sqrt{\frac{r+2R}{r}} + 2K_s[\pi(r+R)-4R]-4\right\}. \quad (1)$$

In addition to bending, the membrane tension (σ) acts on the pore, contributing an elastic energy (E_σ). Therefore, the total energy of the pore is given by

$$E = 2\pi B\left\{\frac{2(r+R)^2}{R\sqrt{r(r+2R)}}\arctan\sqrt{\frac{r+2R}{r}} + 2K_s[\pi(r+R)-4R]-4\right\} + E_\sigma. \quad (2)$$

For fusion to planar lipid bilayers, the area of the system is not constant in the course of fusion pore growth because of free exchange of lipids into a reservoir (the hydrocarbon torus). Because tension in the plasma membrane is much less than tension in the planar lipid bilayer, we can estimate the gain in elastic energy of the membrane as proportional to the decrement of the area of the lipid bilayer ΔS after pore formation:

$$E_\sigma = \Delta S\cdot\sigma, \qquad \text{where} \quad \Delta S = -\pi r^2. \quad (3)$$

This estimation assumes that the walls of the fusion pore are formed from material of the low-tension plasma membrane fluxing across the fusion pore because of the gradient of tension.

In the case of beige mouse mast cell degranulation, there are two alternatives. Usually, plasma membrane is not under tension. Granule membranes, however, are thought to be stretched over their granular contents and may be under significant tension (Monck et al., 1990), although under conditions of hyperosmotic shrinkage they can be made flaccid (Zimmerberg et al., 1987). For stretched granular membranes, we use Eq. 3 for E_σ. The justification is similar to the cell-planar bilayer fusion pore. We consider the material for the wall of the fusion pore to be contributed by the plasma membrane as the flux of material across the fusion pore is from the low-tension plasma membrane to the high-tension granule membrane. We thus conceptualize that a hole of radius r forms in the granular membrane with

the original small area πr^2 absorbed into the remainder of the granular membrane. For r small compared to the granule radius, tension will remain approximately constant (for small granules this approximation fails as r increases, although small granules tend to have smaller initial pores) (Spruce et al., 1990; Lollike et al., 1995). This absorption of membrane therefore yields an energy $-\sigma\pi^2$. For flaccid membranes, we use $E_\sigma = 0$, because tension is practically zero in both membranes.

When $K_s = 0$ and $\sigma = 0$, E_0 has a particularly simple form:

$$E_0 = 2\pi B\left\{\frac{2(r+R)^2}{R\sqrt{r(r+2R)}}\arctan\sqrt{\frac{r+2R}{r}} - 4\right\}. \quad (4)$$

E_0 is a homogeneous function of R and r, given as a function of the ratio $\rho = r/R$ (Fig. 3). E_o has a minimum at $\rho = \rho_m \cong 0.6$. The bottom of the canyon, described by $r = \rho_m R$, has constant energy E_0 (Eq. 4). The existence of the canyon is also the dominant feature for nonzero K_s and σ, as described below. It can be shown that the K_s-dependent term in the energy from Eq. (2) is equal to $4\pi BRK_s$ at the bottom of the canyon. Thus only negative K_s leads to energy decreasing at the bottom of the canyon with increasing r, R, a requirement for pore growth.

Pore evolution is determined by pore energetics and mobilities in the r and R directions. We first consider how the energy of the pore varies as a function of r and R. Nonzero values of E_σ and K_s affect the energy profiles in different manners. Rather than consider the most general case, we analyze each situation separately.

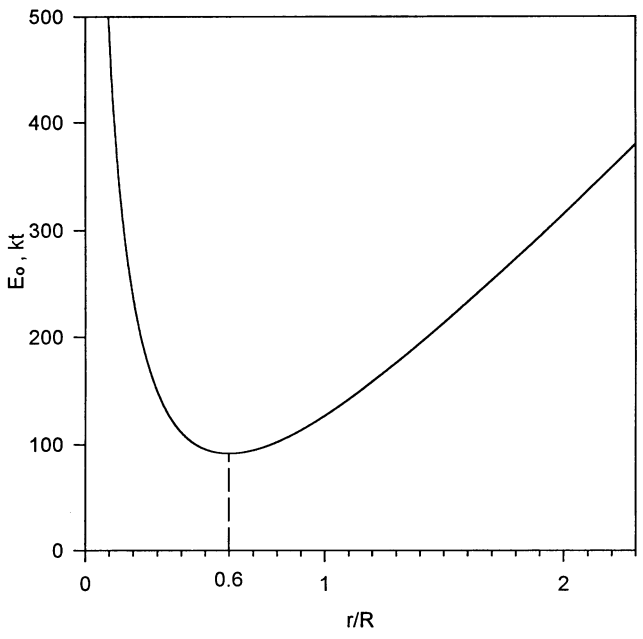

FIGURE 3 Energy E_0 of the fusion pore as a function of the ratio of width/length, $\rho = r/R$, for the case of zero spontaneous curvature ($K_s = 0$) and $\sigma = 0$. In this case the energy is entirely bending energy (Eq. 4). The minimum is located at $\rho_m \cong 0.6$.

Case A: $\sigma \neq 0$, $K_s = 0$

The canyon with flanking energy barriers is illustrated by a three-dimensional plot of $E(r, R)$ in Fig. 4. For this figure, and others, we use $B = 10^{-19}$ J, $\sigma = 5 \times 10^{-4}$ J/m^2 as standard values for bilayers (Evans and Skalak, 1980). The contours of constant energy are shown in Fig. 5 as solid lines, 50 kT apart, and as dotted lines, 10 kT apart. The family of all curves orthogonal to the contours of constant energy are described by (Kreyszig, 1993)

$$\frac{dr}{dR} = -\frac{\partial E/\partial r}{\partial E/\partial R}. \quad (5)$$

The curve of steepest descent, described by Eq. 5, passing through the point $(r, R) = (0,0)$, is the bottom of the canyon (Fig. 4, *dotted line*). The cross sections of the energy profiles for three values of R are shown in Fig. 6. The steepness and height of the energy barrier decrease as R increases. When $R = 14$ nm, the barrier vanishes. The decline of the bottom of the canyon (i.e., the energy minima) with increasing R is also seen in Fig. 6. The energy minima decrease with increases in R at about 6 kT/nm.

Case B: $\sigma = 0$, $K_s < 0$

Cross sections of the energy profiles for three values of R are shown in Fig. 7, using a value of K_s chosen to optimize the pore geometry shown in the cross section of Fig. 2 (Kozlov and Markin, 1987). As in case A, the canyon declines with increasing R and bends toward increasing r. But for any given R there is not an energy maximum (Fig. 7); the energy rises indefinitely for increasing r. However, as R increases, the slope of the energy (in the direction of rising r) decreases. This slope becomes zero for $R = R_f$ and

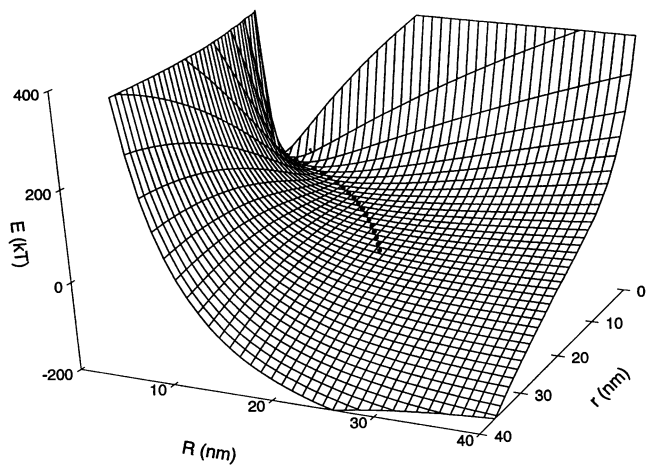

FIGURE 4 Three-dimensional plot of fusion pore energy E (Eqs. 2 and 3) as a function of (r, R) for the case of nonzero tension and zero spontaneous curvature. The function is a "canyon" with steep walls for small (r, R). These walls become shallow as (r, R) increases. The dotted line is the path of minimum energy ("bottom" of the canyon). Parameters are $B = 10^{-19}$J, $\sigma = 5 \times 10^{-4}$J/m^2, and $K_s = 0$.

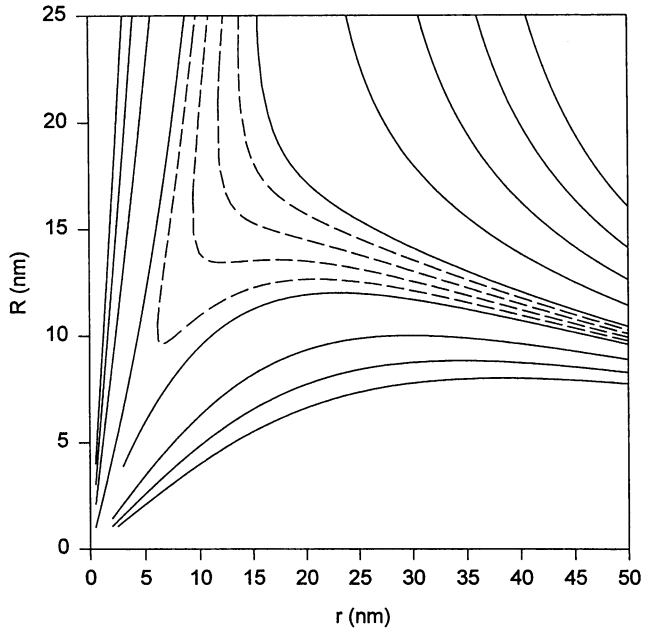

FIGURE 5 Topographic plot of fusion pore energy E (Eqs. 2 and 3) for nonzero tension and zero spontaneous curvature. We first show pairs of solid lines of constant energy 200, 150, 100, and 50 kT, starting near each axis. Next, connected dashed single lines show constant energy of 40, 30, 20, and 10 kT at larger (r, R). Finally, solid lines show 0, -50, -100, -150, and -200 kT at the largest (r, R). Parameters are $B = 10^{-19}$J, $\sigma = 5 \times 10^{-4}$J/m^2, and $K_s = 0$.

negative for $R > R_f$, accounting for the rapid expansion of pores. From Eq. 1, we obtain the linear asymptote for large r

$$E_b = 2\pi^2 Br\left(\frac{1}{2R} + 2K_s\right), \tag{6}$$

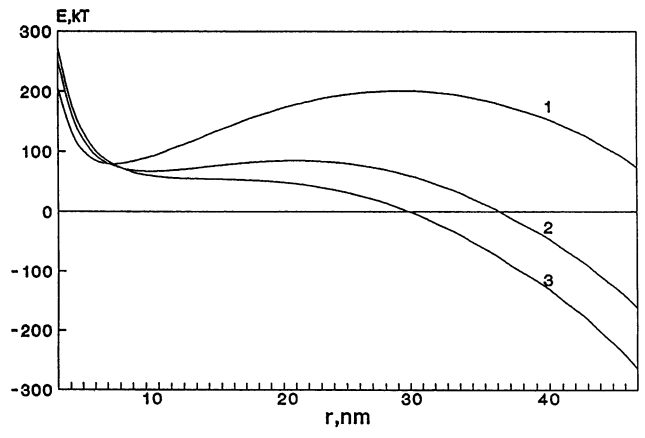

FIGURE 6 Fusion pore energy E (Eqs. 2 and 3) for the case of nonzero tension and zero spontaneous curvature, as a function of r at different constant values of R: 1–10 nm; 2–12.5 nm; 3–14 nm. There no longer is an energy barrier to pore widening at $R = 14$ nm. Parameters are $B = 10^{-19}$J and $\sigma = 5 \times 10^{-4}$J/m^2.

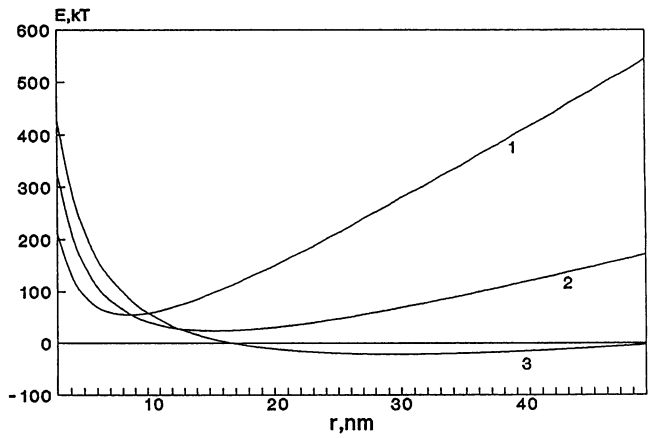

FIGURE 7 Fusion pore energy E (Eq. 3) for the case of $\sigma = 0$ and negative spontaneous curvature, as a function of r at different values of R: 1–10 nm; 2–14 nm; 3–18 nm. The energy barrier vanishes at $R = -1/4K_s$. Parameters are $B = 10^{-19}$J and $K_s^{-1} = -80$ nm.

and thus the barrier vanishes at

$$R_f = -\frac{1}{4K_s}. \tag{7}$$

It is clear from Eq. 6 that positive K_s increases the slope of the canyon and prevents the motion of the pore in the r direction.

Kinetic equations

We treat the orthogonal coordinates of the pore, r and R, as stochastic variables and define $f(t, r, R)$ as the probability density function for the pore to have dimensions r and R at time t. The energy profiles described above determine the evolution of $f(t, r, R)$ according to the Fokker-Planck equation (Kubo et al., 1991):

$$\frac{\partial f}{\partial t} = D_R \frac{\partial^2 f}{\partial R^2} + D_r \frac{\partial^2 f}{\partial r^2} + \frac{D_R}{kT}\frac{\partial}{\partial R}\left(f\frac{\partial E}{\partial R}\right) + \frac{D_r}{kT}\frac{\partial}{\partial r}\left(f\frac{\partial E}{\partial r}\right), \tag{8}$$

where D_R and D_r are the diffusion coefficients for the variables R and r, respectively. The first two terms in the right-hand side of Eq. 8 describe diffusion of the pore in (r, R)-space, and the last two terms describe motion of the pore under the influence of an external force. We refer to this latter motion as "migration." In fact, Eq. (8) has been applied and justified for pores in thin films under the assumption D_r = constant, D_R = constant (Deryaguin and Gutop, 1962).

Diffusion is insignificant compared to migration for both r and R, because the ratio of the migration and diffusional terms is approximately $\Delta E/kT$, where ΔE is the change of energy on a characteristic length during pore evolution. As discussed for cases A and B in Appendices 1 and 3 (also Figs. 6 and 7), $\Delta E \gg kT$. Thus, migration dominates in all domains of the energy profile along both the bottom of the

canyon and the flanking energy barriers. With only migration, Eq. 8 reduces to

$$\frac{\partial f}{\partial t} = \frac{D_R}{kT}\frac{\partial}{\partial R}\left(f\frac{\partial E}{\partial R}\right) + \frac{D_r}{kT}\frac{\partial}{\partial r}\left(f\frac{\partial E}{\partial r}\right). \quad (9)$$

It is easy to show (Kubo et al., 1991) that the average values $\bar{r}$, $\bar{R}$ calculated with the distribution function f from Eq. 8 satisfy the following equations:

$$\frac{d\bar{R}}{dt} = -\frac{D_R}{kT}\overline{\frac{\partial E}{\partial R}} \qquad \frac{d\bar{r}}{dt} = -\frac{D_r}{kT}\overline{\frac{\partial E}{\partial r}}.$$

If the initial distribution is a δ-function (fixed values of radii), then in the absence of diffusion the distribution function remains a δ-function for all times. In this case R and r migrate along the characteristics of Eq. 8 given by

$$\frac{dR}{dt} = -\frac{D_R}{kT}\frac{\partial E}{\partial R} \qquad \frac{dr}{dt} = -\frac{D_r}{kT}\frac{\partial E}{\partial r}. \quad (10)$$

Phase plane analysis of pore dynamics

When analytical solutions of differential equations such as Eq. 10 are not possible, phase plane methods are particularly useful (Kreyszig, 1993). They allow the qualitative dynamic features of the solutions to be obtained, without having to actually solve the system of equations. Because the right-hand sides of Eq. 10 are nonlinear functions of r, R, analytical solutions do not exist.

To obtain fusion pore dilation in stages, we assume that the mobility of r is greater than that of R. Possible origins of the inequality $D_r \ll D_R$ are considered in the Discussion. Because the energetics of pore formation and pore evolution are different, the initial r and R would not be expected to lie in the bottom of the canyon, i.e., $\partial E/\partial r$ is initially far from zero. The pore immediately falls to the bottom of the canyon by rapidly changing r, with R remaining relatively constant. Thus the pore rapidly approaches dimensions at which $\partial E/\partial r \cong 0$. Because $\partial E/\partial r$ is now small, the pore dynamics are limited by the rate at which R increases. The large mobility in the r dimension ensures that the pore migrates with minimal $\partial E/\partial r$. Along this resultant curve, which approximates the true trajectory, Eq. 10 can be reduced to a single differential equation for $R(t)$ and an algebraic equation (because $\partial E/\partial r = 0$) for $r(t)$. Because motion along this curve is limited by the slower of the two mobilities, it is referred to as the "slow curve."

The exact set of numerically generated trajectories on the plane (r, R) obtained for $D_R/D_r = 2 \times 10^{-2}$ (Fig. 8, *solid curves*) can be compared to the slow curve $\partial E/\partial r = 0$ (curve 1) and the curve of steepest descent (curve 2). For reference, the bottom of the canyon for the energy E_0 is also given (curve 3). In the domain of small (r, R), curves 1, 2, and 3 remain close to each other. They diverge as r, R increases. The slow curve best approximates the exact curve both when $\sigma \neq 0$, $K_s = 0$ (Fig. 8 *A*) and $\sigma = 0$, $K_s < 0$ (Fig. 8 B). For small initial radius r, the pore quickly rolls down to

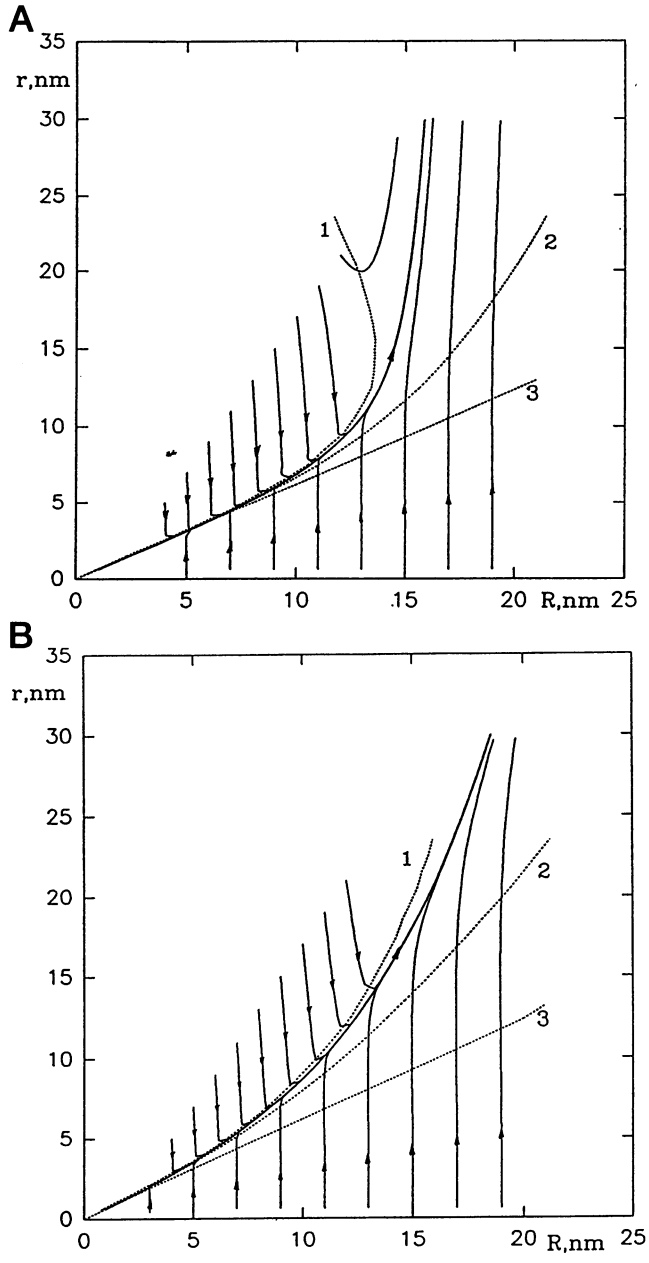

FIGURE 8 Phase curves of system of Eq. 10 for the case of (*A*) nonzero tension and zero spontaneous curvature and (*B*) $\sigma = 0$ and negative spontaneous curvature. The dotted curve 1 is the slow curve $\partial E/\partial r = 0$. Dotted curve 2 is the gradient curve (the bottom of the canyon). Dotted line 3 is the bottom of the canyon for nondisturbed case (homogeneous energy). (*A*) Parameters are $D_r = 10^{-12}$ cm²/s, $D_R = 2 \times 10^{-14}$ cm²/s, $B = 10^{-19}$J, and $\sigma = 5 \times 10^{-4}$J/m². (*B*) Parameters are $D_r = 10^{-12}$ cm²/s, $D_R = 2 \times 10^{-14}$ cm²/s, $B = 10^{-19}$J, and $K_s^{-1} = -80$ nm.

the slow curve and thereafter migrates along it, with the rate defined by D_R/kT, predicting the experimentally observed semi-stable values of conductance for extended times. Eventually the slow curve appreciably bends in the direction of increasing r (Fig. 8), experimentally seen as a pore with a more rapidly enlarging conductance. In the limiting case of $D_R/D_r \Rightarrow 0$ and $\sigma \neq 0$ (Fig. 8 *A*), the system becomes unstable at the point where the tangent of the slow curve is

vertical. After this point the pore breaks from the slow curve and r rushes to infinity. When D_R/D_r is small, not quite zero, the true phase curve starts to deviate below the slow curve before the breaking point and the transition to rapid increases in r occurs gently. In the case $\sigma = 0$, $K_s < 0$ (Fig. 8 *B*), the slow curve only asymptotically achieves a vertical tangent (for values of r, R larger than shown). As a consequence, for $D_R/D_r \ll 1$ the pore remains on the slow curve for prolonged times. Because the slow curve (Fig. 8 *B*, *curve 1*) declines in the direction of increasing r, the pore diameter enlarges slowly. In summary, for both cases ($\sigma \neq 0$, $K_s = 0$ and $\sigma = 0$, $K_s < 0$), when D_R/D_r is small but nonzero, the true trajectory of motion and the slow curve gradually, but increasingly, diverge. As the divergence occurs, a transition to rapid motion takes place.

We numerically integrated Eq. 10 to calculate the trajectories and conductances of fusion pores. But as analytical approximations are convenient to appreciate pore dynamics, we also used a perturbation theory to estimate pore expansion rates and pore lifetimes when D_R/D_r is small.

ANALYTICAL APPROXIMATIONS TO PORE DYNAMICS

Initial pore widening

Our description begins immediately after formation of the initial pore. The energy E of the small initial pore can be significantly greater than that at the minimum of the r cross section of the energy profile at constant R. Asymptotically, we obtain from Eq. 2 for small r

$$E = 2\pi^2 B\sqrt{R/r}. \tag{11}$$

Because $\partial E/\partial r \gg dE/\partial R$, and $D_r \gg D_R$, the motion along R can be neglected. From Eqs. 10 and 11, the growth of the pore is given by

$$\frac{dr}{dt} = \gamma\sqrt{R}r^{-3/2}$$

where $\gamma = \pi^2 BD_r/kT$. The characteristic time for the pore to relax into an energy minimum is

$$\tau_1 \cong \frac{2}{5\gamma\sqrt{R}} r_1^{5/2}, \tag{12}$$

where r_1 is the radius once the pore is at a minimum energy ($r_1/R = \rho_m = 0.6$). Experimentally, τ_1 is fast, at most several milliseconds. For an initial value of R equal to R_i = 10 nm and $B = 10^{-19}$ J, we need to assume $D_r \geq 10^{-12}$ cm^2/s to match experiments.

Slow pore growth

Case A: $\sigma \neq 0$, $K_s = 0$

The slow curve (Fig. 8 *A*, *curve 1*), the curve of steepest descent (*curve 2*) and the curve describing the bottom of the canyon when $\sigma \neq 0$, $K_s = 0$ (*curve 3*) are close to each other and to the true curve of migration (*solid curves*) for small r and R. During the semi-stable stage the fusion pore moves along the slow curve $\partial E/\partial r = 0$. This allowed us to approximate the phase curve using a perturbation expansion and to calculate the consequent pore migration (Appendix 1). The height of the energy barrier (W) that confines the pore to the slow curve is approximately Eq. A1.11,

$$W = \pi^2 B(\pi B/4\sigma R^2 - \rho_m). \tag{13}$$

W is reduced from about 10^{-18}J $\cong$ 200 kT at $R_i \cong$ 10 nm to ≈ 0 at R_f = 16 nm, for $B \cong 10^{-19}$ J, $\sigma \cong 5 \times 10^{-4}$ J/m^2. Thus the energy barrier decreases as R increases. When R becomes sufficiently large (i.e., the pore has become long) there is no energy barrier inhibiting expansion and the pore will rapidly enlarge. This analytic approximation overestimates the true energy barrier. The numerically correct evaluation is given in Fig. 6, where it can be seen that W = 125 kT for R_i = 10 nm and $W \approx 0$ for R_f = 14 nm.

The time for the pore to grow from R_i to R_f can be calculated from the first equation of system 10, utilizing Eqs, A1.4 and A1.6:

$$\frac{dR}{dt} = \frac{D_R}{kT} 2\pi\rho_m^2\sigma R.$$

Integrating this equation yields

$$R = R_1 \exp(2\pi\rho_m^2\sigma D_R t/kT). \tag{14}$$

The time, τ_2, that the pore remains in the semistable stage is

$$\tau_2 = (kT/2\pi\rho_m^2\sigma D_R)\ln(R_f/R_i). \tag{15}$$

Using the usual values for the parameters and letting $D_R \cong 10^{-15}$ cm^2/s, with $R_i \cong$ 10 nm, $R_f \cong$ 15 nm, we get $\tau_2 \cong$ 5 s, in accord with the mean lifetime in the S stage for cell-planar membrane fusion (Fig. 1 *B*).

Superimposed on the dynamical motion of the pore along the canyon are rapid fluctuations of r across the canyon. These occur because the ratio D_r/D_R is high and the derivative $\partial E/\partial r$ is much steeper on the barriers flanking the canyon than along the canyon. These fluctuations could account for the rising and falling conductance observed during the semi-stable stage (see Fig. 1). Although fluctuations can overcome the low barriers occurring for large R, causing pores to leave the S stage, fluctuations are not the major determinants for the lifetimes of pores in this stage (Appendix 2, Fig. 13).

Case B: $\sigma = 0$, $K_s < 0$

Expansion caused by a negative spontaneous curvature of the membrane forming the neck of the pore can be solved by a method similar to that of case A (Appendix 3). When D_r/D_R is large the pore moves along the slow curve given by $\partial E/\partial r = 0$ (Fig. 8 *B*, *curve 1*). As shown in Appendix 3 the

change in energy ΔE as the pore migrates from R_i to R_f is given by Eq. A3.3:

$$\Delta E = 4\pi^2 \rho_m K_s B (R_f - R_i). \quad (16)$$

R_f is given by Eq. 7:

$$R_f = -\frac{1}{4K_s}.$$

Using $R_i = 10$ nm, $K_s^{-1} = -80$ nm^{-1}, $B = 10^{-19}$ J, we get $\Delta E \cong 3 \times 10^{-19}$ J $\cong 75kT$. Thus, in this case we can again ignore the diffusional terms of Eq. 8. Taking Eq. 10 in the form of finite differences and using ΔE from Eq. 16 yields the lifetime of the semistable state

$$\tau_2 = \frac{kT}{D_R}\left(\frac{1}{4K_s} + R_i\right)(4\pi^2 \rho_m K_s B)^{-1}. \quad (17)$$

We obtain $\tau_2 \cong 0.08$ s for $R_i = 10$ nm, $K_s^{-1} = -80$ nm, $B = 10^{-19}$ J, $D_R = 2 \times 10^{-13}$ cm^2/s, in accord with Fig. 1 *A*, for exocytosis. Because the energy barrier is not bounded in this case (see Fig. 7), rapid fluctuations cannot change the time the pore remains in the semi-stable stage.

The distribution of lifetimes in the semi-stable stage

For both mast cell secretion (Fig. 9; see also Monck et al., 1990) and HA-expressing cell to bilayer fusion (Melikyan et al., 1993a), the lifetimes of the pores in the semi-stable stage are exponentially distributed. With the present description of fixed initial parameters, the lifetimes are not distributed; rather, they are unique. Our model is easily generalized to nonfixed parameters. We illustrate by letting the initial R, R_i be distributed with probability density function $g(R_i)$ and calculate the resulting distribution of lifetimes. We use Eq. 14 to relate R_f and R_i:

$$R_i = R_f \exp(-at),$$

where $a = 2\pi\rho_m^2 \sigma D_R / kT$. We obtain the probability density of lifetimes, $F(t)$, as

$$F(t)dt = g[R_i(t)]\left|\frac{dR_i}{dt}\right| dt = aR_f \exp(-at) g[R_i(t)]dt.$$

R_f is not stochastic in this treatment. It is set by the length of the pore when the energy barrier $W = 0$ (Eq. 13). For simplicity we let $g(R_i)$ be uniformly distributed for R_i between some value R_g (the minimal initial R, set by geometrical characteristics of the membranes) and R_f:

$$g(R_i) = \begin{cases} 0 & \text{for } R_i < R_g \\ (R_f - R_g)^{-1} & \text{for } R_g \leq R_i \leq R_f \\ 0 & \text{for } R_i > R_f. \end{cases}$$

This yields $F(t) = aR_f(R_f - R_g)^{-1}\exp(-at)$ for $t < t_g = a^{-1}\ln(R_f/R_g)$, where t_g is the maximal lifetime of the fusion pore in the semistable state, corresponding to $R_g = R_i$. For $t > t_g$, $F(t) = 0$. The probability that the pore has remained in the S stage for time greater than t is

$$P(t) = 1 - \int_0^t F(\tau)\, d\tau = \frac{R_f}{R_f - R_g}[\exp(-at) - R_g/R_f].$$

This distribution $P(t)$ is shown (Fig. 10) for $R_g = 10$ nm, $\sigma = 1.5 \times 10^{-4}$ J/m^2, $B = 10^{-19}$ J, and $D_R = 10^{-15}$ cm^2/s. With these parameters, $a = 0.01$ s^{-1} and $R_f = 30$ nm.

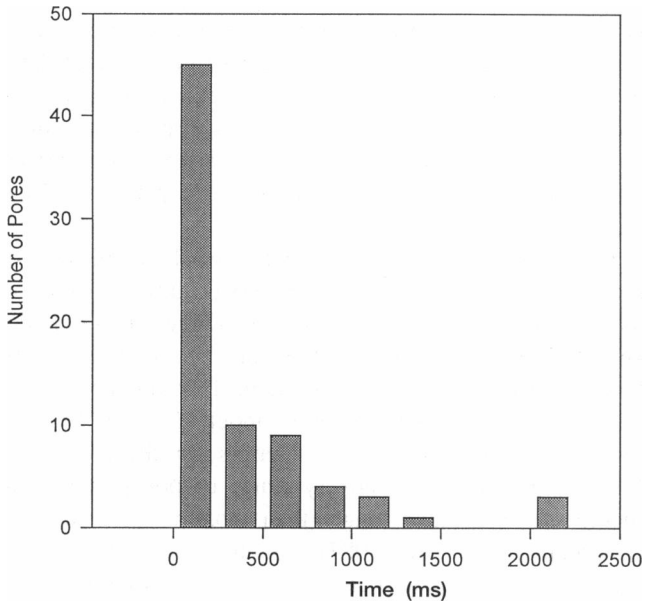

FIGURE 9 Lifetime distribution of semi-stable exocytotic fusion pores of beige mouse mast cells determined by admittance measurements by Curran et al. (1993). Lifetimes of pores were measured from initial pore formation until 20 nS in conductance. Times are given in ms. Distribution fits an exponential distribution ($p < 0.05$) by the WE test (Hahn and Shapiro, 1967).

Final widening of the pore

Case A: $\sigma \neq 0$, $K_s = 0$

After the pore enlarges sufficiently, the energy barrier vanishes and the pore dilates according to the expression for dr/dt in Eq. 10, where the energy is given by $-\sigma\pi r^2$. Integration yields

$$r(t) \cong r(\tau_2)\exp(2\pi\sigma D_r t/kT), \quad (18)$$

where τ_2 is the time at which the pore initiates its rapid widening out of the S stage. The pore radius grows exponentially with a time constant $\tau_3 \approx 10$ ms for $\sigma \cong 5\ 10^{-4}$ J/m^2 and $D_r \cong 10^{-12}$ cm^2/s. Such a rapid rise for final pore widening is observed for cell to planar bilayer fusion.

Case B: $\sigma = 0$, $K_s < 0$

For expansion out of the semi-stable stage, we use the asymptotic form of E_b at large r (Eq. 6). Combining this

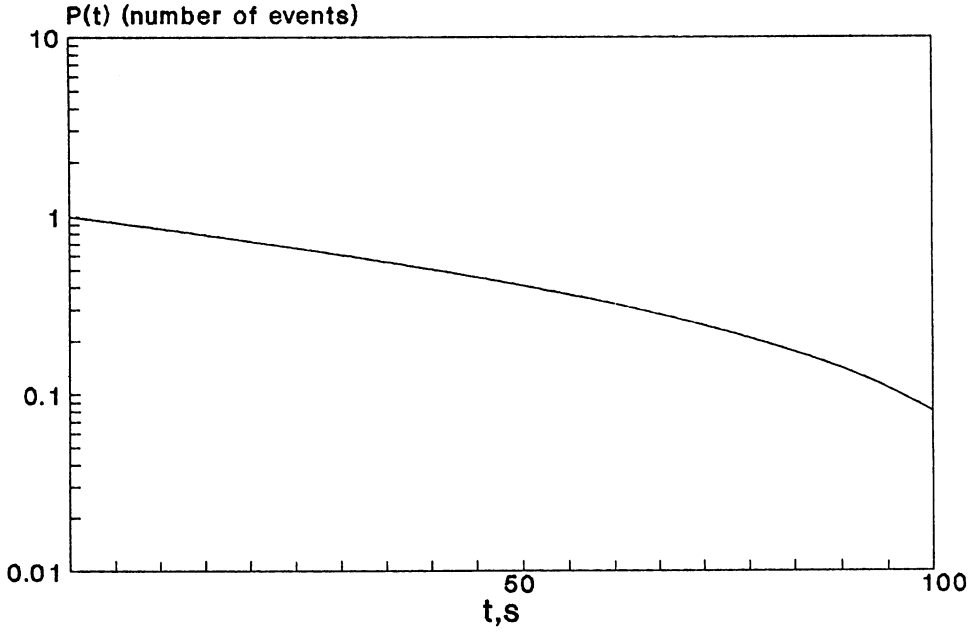

FIGURE 10 Distribution of lifetimes for theoretical fusion pores for the case of nonzero tension and zero spontaneous curvature, with initial external radii, R_i, uniformly distributed between R_g = 10 nm and R_f = 30 nm. Parameters are $\sigma = 1.5 \times 10^{-4}$J/m^2, $B = 10^{-19}$J, and $D_R = 10^{-15}$ cm^2/s.

with Eq. 10 yields the dynamics of the pore as

$$\frac{dr}{dt} = -\frac{D_r}{kT}(4K_s + 1/R)\pi^2 B, \qquad \text{for} \quad R > R_f.$$

The expansion of the pore is thus linear in t. For $B \cong 10^{-19}$ J, $R \cong 25$ nm, $K_s^{-1} \cong -80$ nm, $D_r \cong 10^{-12}$ cm^2/s, r expands at the rate of 250 nm/s. The radius of the pore enlarges twofold (for example, from 25 to 50 nm) in the time interval $\tau_3 \approx 10^{-1}$ s. Note that τ_3/τ_2 is set by the ratio D_R/D_r (see Eq. 17). Experimentally, pore rise times are much slower for exocytosis than for cell-planar bilayer fusion (Fig. 1), in accord with this model. In some experiments, exocytotic fusion pore rise times are faster, perhaps reflecting variability in the degree of granular membrane tension. Hyperosmotic conditions, which relieve granular membrane tension, slow the growth of fusion pores in beige mouse mast cell secretion (Curran and Zimmerberg, unpublished observations).

In short, when $\sigma \neq 0$, the final dilation of pores occurs exponentially. When $\sigma = 0$, spontaneous negative curvatures of membranes will cause pores to enlarge linearly when they leave the semi-stable stage.

DISCUSSION

Stages are due to unequal mobilities

We treated the pore as a symmetrical object described by two dynamical variables. Each configuration of a pore is defined by its radius and its length and is a point in a phase plane. Because mechanical energy greatly changes along trajectories (compared to kT), migration driven by these energy gradients dominates diffusional motion. The pore is thus represented as a quasiparticle responding to force fields with motions determined by mobilities and energy gradients. Stages arise when mobilities of different dynamic variables are unequal and energy minima with respect to the fast variable (r) appear. From the initial state, particles move down energy gradients, with motion occurring predominantly in the direction with the larger mobility. When a particle reaches a position with a zero r-component energy gradient, and therefore zero driving force in this direction, the motion of the particle is redirected along the remaining component of the energy gradient. But as the mobility is smaller in the new direction, changes in position are now slower than prior ones. This slow motion continues until a position in phase space is reached where an energy gradient in the r-component again occurs. The particle alters its direction of motion and rapidly changes its position in the r direction. In essence, energy-driven systems characterized by multiple and unequal mobilities seek paths of "least resistance."

In our model, unequal and rather small mobilities are required to obtain different characteristic times for motion along the canyon and for final pore widening. The small and very different values of D_r and D_R may be accounted for by known physical properties of biological membranes. D_r for a pore in planar lipid bilayer is about 10^{-8}-10^{-9} cm^2/s, much higher than $D_r \sim 10^{-12}$ cm^2/s for the theoretical fusion pore. But the recovery times of pores in plasma membranes are much longer than those in lipid bilayers (Chernomordik et al., 1987), which is attributed to the trapping of membrane proteins and supra-membrane structures by pore edges. Membrane proteins and supra-membrane structures may similarly restrict the r mobility of the fusion pore. The cortical layers and high viscosity of cytoplasm may lead to even smaller D_R. Alternatively, the contacts between opposing membranes may not be confined to the fusion pore alone: there may be additional connec-

tions between membranes that hinder motion in the R direction. The multiplicity of fusion proteins and pores in cell-cell fusion is consistent with this last possibility (Zimmerberg et al., 1994).

Characteristic times are determined by both the mobilities and the energy gradients. But these gradients (the decline of the canyon in the R direction along the slow curve, and the steepness of the energy profile in the r direction at larger R) are determined by the same parameter: σ in case A and K_s in case B. By comparing Eqs. 14 and 18 it is obvious that in case A the ratio $\tau_3/\tau_2 \sim D_R/D_r$. In case B, when widening is linear in time the ratio of the rates (proportional to $1/\tau$) is also D_r/D_R.

We have considered a fusion pore as an object whose energy depends on mechanical bending and tension. For these fusion pores, motion down the steep energy barriers along the high-mobility r direction is responsible for the early fast enlargement. The motion switches direction at dimensions corresponding to the bottom of the canyon. Motion now occurs in the low-mobility R direction as well as the r direction because the bottom of the canyon inclines gently downward and progressively bends toward greater r for increasing R. High-frequency oscillations in the direction of r give rise to fluctuations in conductance (Appendix 2). Motion along the bottom of the canyon is responsible for the stage of the slowly growing, but semi-stable conductances. As R increases, the flanking energy barrier decreases. The pore escapes the canyon, because of a fluctuation over a vanishingly small barrier, with a rapid increase in pore conductance.

This approach runs counter to previous views that did not assign a role to the length in pore expansion (Zimmerberg et al., 1987; Spruce et al., 1990, 1991; Nanavati et al., 1992). By characterizing the pores with two dimensions, stages arise naturally for many geometries and functional forms of energy gradients. However, the precise dynamics are determined by the shape of the energy profile, which is sensitive to tension and spontaneous curvature. The distribution of lifetimes of the semi-stable stage can be accounted for if the initial pore dimensions and the mechanical parameters of the membranes are disperse. This predicted dispersion is consistent with the observation that initial pore conductances are broadly distributed for secretion (Spruce et al., 1990; Curran et al., 1993), viral protein mediated syncytia formation (Spruce et al., 1991; Lanzrein et al., 1993; Plonsky and Zimmerberg, 1994), and cell-planar membrane fusion (Melikyan et al., 1993a). Variations in initial conditions (e.g., in R_i) account for the distribution of lifetimes of the semi-stable stage. Rapid pore widening without a semi-stable stage would occur when the initial values of R_i, B, and σ lead to no significant barrier to pore widening.

The conductance of the pore

Experimentally observed fusion pores are characterized by three stages: a quick rise, a relatively prolonged time period with conductances within a narrow range that defines the semi-stable stage, and a more rapidly enlarging final phase (Curran et al., 1993; Melikyan et al., 1993a). This paper presents a natural physical mechanism for such behavior. We illustrate the increase of conductance, G, in time using the simplest expression, $G = (\pi r^2/2R)g$ for a cylindrical pore, where g is the specific conductance. The difference in conductance between a cylindrical and toroidal pore (Nanavati at al., 1992) is small: the latter exceeds the former by a factor of 1.4 once the pore is at the bottom of canyon, with the difference tending to zero as the pore enlarges. Pore growth is sensitive to the membrane parameters, which we illustrate for the case $\sigma > 0$ (Fig. 11). A twofold increase in σ results in a 20-fold decrease in the lifetime of the semi-stable stage and a 20-fold increase of the slope of the G–t curve. This occurs primarily because the characteristic length over which the energy barrier is lowered varies inversely with $\sqrt{\sigma}$ (Eq. 13), secondarily because the slope along the canyon is increasing with σ. The fast relaxation time for the final increase of $G(t)$ also depends on σ (Eq. 18). The bending elasticity, B, affects the shape of the $G(t)$ curve and the lifetime of the semi-stable stage in a manner

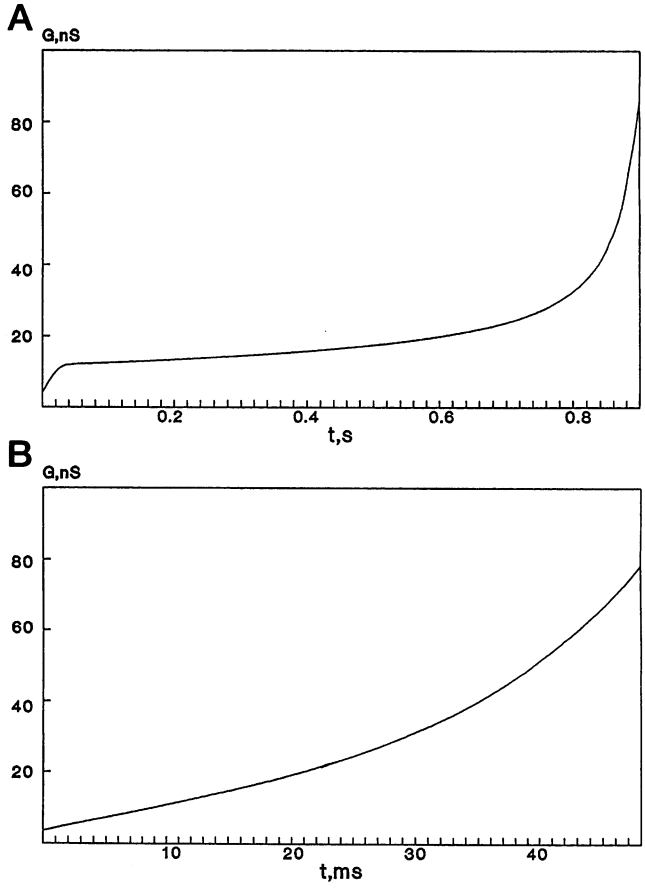

FIGURE 11 Sensitivity of fusion pore evolution to a doubling of tension for the case of nonzero tension and zero spontaneous curvature. (*A*) Conductance $G(t)$ in time of a cylindrical pore with parameters $D_r = 10^{-12}$ cm^2/s, $D_r/D_R = 50$, $B = 10^{-19}$J, $\sigma = 5 \times 10^{-4}$J/m^2, and $g = 2$ nS/nm. (*B*) Conductance in time for identical parameters except $\sigma = 10^{-3}$J/m^2.

(and for reasons) similar to that discussed for tension. For example, a twofold decrease in B leads to a greater than 10-fold decrease in the lifetime of the semi-stable stage with a proportional decrease in the slope of $G(t)$. The effects of D_r and D_R on lifetimes and rise times are straightforward and have a purely kinetic mechanism.

When $\sigma = 0$, $K_s < 0$, after rolling down to the bottom of the canyon the pore moves approximately along the slow curve $\partial E/\partial r = 0$. Gradually and increasingly this curve deviates from the true trajectory, which predicts a smooth increase of radius r and conductance G (Fig 12). Varying the spontaneous curvature, K_s alters the incline of $G(t)$ during the semi-stable stage as well as the final rise upon leaving this stage. This rise is slower than the exponential rise predicted for $\sigma \neq 0$ and could account for the slower rise of conductance usually seen for mast cell fusion pores (Curran et al., 1993) compared to cell-planar membrane fusion pores (Melikyan et al., 1993b) after they leave the semi-stable stage.

The theoretical model is an oversimplification. First, the pore is not exactly toroidal, being hourglass shaped with two dimples on the fusing membranes and a narrow tube connecting them. Second, elastic energy was introduced in its simplest form. It ignores both the real shape and the distribution of tension along the walls of the fusion pore. However, it does provide a reasonable approximation when only one of the fusing membranes is under significant tension. The general case requires separate and dedicated considerations. Third, the two fusing membranes usually will have different chemical compositions, tensions, and spontaneous curvatures, resulting in lipidic flow, ignored in the model (Monck et al., 1990). Fourth, the role of cytoskeleton is not considered. Fifth, D_R and D_r were assumed to be constant, which probably is not strictly valid. Despite these limitations, several general features of experimental fusion pores are accounted for by a simple mechanical model with two dynamical variables.

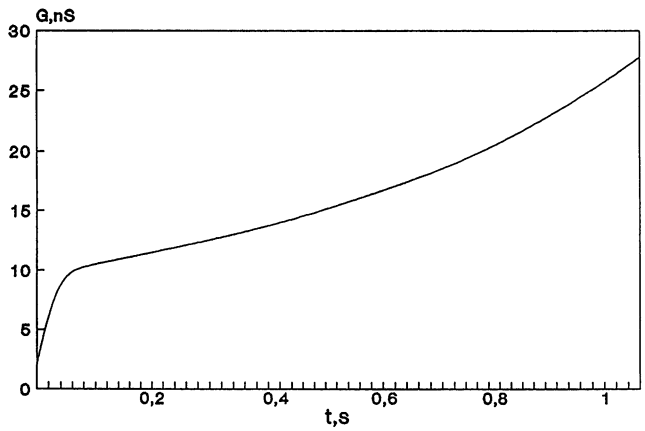

FIGURE 12 Conductance $G(t)$ in time of a theoretical cylindrical fusion pore for the case of $\sigma = 0$ and negative spontaneous curvature. Parameters are $D_r = 10^{-12}$ cm^2/s, $D_r/D_R = 50$, $B = 10^{-19}$J, $K^{-1}{}_s = -80$ nm, and $g = 2$ nS/nm.

APPENDIX 1

Phase trajectory and energy barrier in Case A ($\sigma \neq 0$, $K_s = 0$)

We defined the dimensionless quantity $\epsilon = \sigma r_*^2/2B$ (ratio of energy of tension to bending energy) where r_* is a radius of the pore about 10 nm, corresponding to $G \approx 20$ nS. If $\sigma = 5 \times 10^{-4}$ J/m^2, $B = 10^{-19}$ J we obtain $\epsilon = 0.25$. To first order in ϵ:

$$r = r_0(R) + \epsilon r_1(R), \tag{A1.1}$$

where $r_0(R) = \rho_m R$. From the condition $\partial E/\partial r = 0$ where $E = E_0 - \pi\sigma r^2$,

$$\frac{\partial E_0}{\partial r} - B\frac{4\pi\epsilon}{r_*^2} r = 0. \tag{A1.2}$$

But, to first order in ϵ,

$$\frac{\partial E_0}{\partial r} = \frac{\partial E_0}{\partial r}\bigg|_{r_0} + \frac{\partial^2 E_0}{\partial r^2}\bigg|_{r_0} \epsilon r_1 = \frac{\epsilon}{R^2}\alpha r_1, \tag{A1.3}$$

where $\alpha = \partial^2 E_0/\partial\rho^2|_{\rho m}$. From Eqs. A1.2 and A1.3,

$$r_1 = B\frac{4\pi R^2 r_0}{r_*^2 \alpha} = \frac{4\pi\rho_m R^3}{r_*^2\,\alpha} B. \tag{A1.4}$$

Eq. A1.4 gives the phase curve to first order in ϵ. The change in energy, ΔE, in the region of slow motion, between R_i and R_f can be obtained to first order in ϵ:

$$\Delta E = \frac{\partial E}{\partial r}\Delta r + \frac{\partial E}{\partial R}\Delta R. \tag{A1.5}$$

Along the slow curve we have $\partial E/\partial r = 0$ and only the derivative $\partial E/\partial R$ need be calculated:

$$\frac{\partial E}{\partial R}\bigg|_{r(R)} = \frac{\partial E_o}{\partial R}\bigg|_{r(R)}.$$

Using Eq. A1.1,

$$\frac{\partial E}{\partial R}\bigg|_{r(R)} = \frac{\partial E_0}{\partial R}\bigg|_{r_o} + \frac{\partial^2 E_0}{\partial R \partial r}\bigg|_{r_o} r_1(R).$$

But

$$\frac{\partial E_0}{\partial R}\bigg|_{r_o} = 0 \quad \text{and} \quad \frac{\partial^2 E_0}{\partial R \partial r}\bigg|_{r_0} = \frac{\partial^2 E_0}{\partial \rho^2}\bigg|_{\rho_m} \frac{\partial \rho}{\partial r}\bigg|_{r_0} \frac{\partial \rho}{\partial R}\bigg|_{r_0},$$

yielding

$$\frac{\partial E}{\partial R}\bigg|_{r(R)} = -\epsilon\frac{\alpha r_0}{R^3} r_1(R). \tag{A1.6}$$

Substituting Eq. A1.4 into Eq. A1.6 and using Eq. A1.5 we get

$$\Delta E = -2\pi\rho_m^2 \sigma R_1 (R_f - R_i). \tag{A1.7}$$

Assuming $R_i = 10$ nm, $\sigma = 5 \times 10^{-4}$ J/m^2, and $R_f = 15$ nm yields $\Delta E \cong 25\ kT$. This is in accordance with Fig. 6 and justifies ignoring the diffusional terms of the Fokker-Planck equation.

It is useful to derive an analytic form for the height of the energy barrier, W. From Eq. 1, for large r we have (for $K_s = 0$) for fixed R:

$$E_0 = \frac{\pi^2 B}{R} r. \tag{A1.8}$$

The energy $E_0 - \pi\sigma r^2$ is maximal (E_M) for

$$r_M = \pi B/2\sigma R. \qquad \text{(A1.9)}$$

When $r > \rho_m R$ we use Eq. A1.8 to obtain

$$E = E_m + (r - \rho_m R)\pi^2 B/R - \pi\sigma r^2, \qquad \text{(A1.10)}$$

where E_m is the minimum value of energy. From Eqs. A1.9 and A1.10 we have for the height of the barrier $W = E_M - E_m$:

$$W = \pi^2 B(\pi B/4\sigma R^2 - \rho_m). \qquad \text{(A1.11)}$$

APPENDIX 2

Fluctuations of the pore in Case A ($\sigma \neq 0$, $K_s = 0$)

The probability that the pore overcomes the energy barrier W in a time dt is $\nu \exp(-W(t)/kT)dt$, where ν is the characteristic frequency of the fluctuations. We describe the probability density function, $f(t)$, for the pore remaining in the S stage at time t by the standard methods of stochastic theory:

$$f(t) = f(0)\exp\left[-\nu\int_0^t \exp(-W(\tau)/kT)\,dt\right]. \qquad \text{(A2.1)}$$

We estimate $f(t)$ using Eq. A1.11 for W and Eq. 14 for $R(t)$:

$$f(t) = f(0)\exp\left\{-\nu\exp\left(\frac{\pi^2\rho_m B}{kT}\right)\right.$$
$$\left.\int_0^t \exp\left\{-\frac{\pi^3 B^2}{4kT\sigma R_i^2}\exp\left\{-\frac{4\pi\rho_m^2\sigma D_R}{kT}\tau\right\}\right\}d\tau\right\}.$$

After integration we obtain

$$f(t) = f(0)\exp\left\{-\nu\frac{e^p}{g}[\mathrm{Ei}(-he^{-gt}) - \mathrm{Ei}(-h)]\right\},$$

where $p = \pi^2 B\rho_m/kT$, $g = (4\pi\rho_m{}^2/kT)\sigma D_R$, $h = \pi^3 B^2/4kT\sigma R_i{}^2$, and Ei is the integral exponential function. For $B = 10^{-19}$ J, $\sigma = 5 \times 10^{-4}$ J/m^2, $D_R = 2 \times 10^{-14}$ cm^2/s, $R_0 = 10^{-8}$ m we have $p \cong 140$, $g \cong 1$ s^{-1}, $h \cong 380$. As the argument of Ei is large we use the asymptotic expression: $\mathrm{Ei}(-x) = -e^{-x}/x$. We obtain

$$f(t) = f(0)\exp[-\nu(gh)^{-1}[\exp(p + gt - he^{-gt}) - \exp(p - h)]]. \qquad \text{(A2.2)}$$

$f(t)$ has the form of a rounded step function; the ratio $f(t)/f(0)$ differs from 1 or 0 for only a small time interval. The position of the transition is determined by the frequency ν (e.g., increased ν leads to decreased mean lifetime). We estimate this frequency as $\nu \cong D_r/l^2$, where l is the characteristic length. If l is on the order of Δr, which can be estimated from Fig. 1 as ~1 nm, we have $\nu \approx 5 \times 10^2$ s^{-1}, for $D_r = 10^{-12}$ cm^2/s. According to Eq. A2.2, using $\nu = 5 \times 10^2$ s^{-1}and parameters p, g, h as estimated above, we obtain $t_{1/2} \sim 1$ s, where $f(t_{1/2})/f(0) = 0.5$. Eq. A2.2 is a rough approximation because Eq. A1.11 is a simplified form for the height of the energy barrier. Therefore we numerically calculated $f(t)/f(0)$ using Eq. A2.1 and the precise energy barrier W. The function $f(t)/f(0)$ is shown by the solid lines for two values of ν, $\nu = 10^3$ s^{-1} and $\nu = 10^5$ s^{-1} (Fig. 13). The true step function (the dotted lines) shows the time for the height of the barrier to fall to zero. As expected, the more frequent the fluctuations the shorter the lifetime. But this shortening is small compared to the overall lifetime.

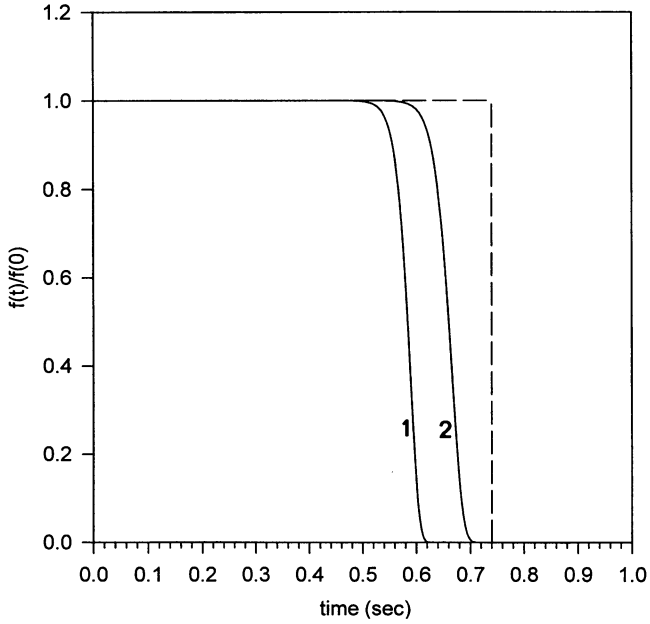

FIGURE 13 Probability density $f(t)/f(0)$ of the distribution of ages t of theoretical fusion pores for the case of nonzero tension and zero spontaneous curvature. The dashed line corresponds to the pure dynamical evolution (no fluctuations). (*1*) $D_r = 10^{-12}$ cm^2/s, $D_r/D_R = 50$, $B = 10^{-19}$J, $\sigma = 5 \times 10^{-4}$J/m^2, and fluctuation frequency $\nu = 10^5$ s^{-1}. (*2*) Same parameters except $\nu = 10^3$ s^{-1}. More frequent fluctuations tend to diminish pore lifetimes.

APPENDIX 3

Phase trajectory for Case B ($\sigma = 0$, $K_s < 0$)

We estimate the variation of energy, E, along the slow curve from a perturbation approach using the expansion parameter $\epsilon = -K_s r_*$, where r_* is the characteristic radius of the pore. For $K_s^{-1} = -80$ nm, $r_* = 10$ nm, $\epsilon = 0.12$, making a perturbation approach reasonable. We rewrite Eq. 1 in the form $E = E_0 - 4\pi(\epsilon/r_*)[\pi(r + R) - 4R]B$. We determine the line $\partial E/\partial r = 0$ by using $r = r_0 + \epsilon r_1$. In place of Eq. A1.2 we have

$$\frac{\partial E_o}{\partial r} - 4\pi^2\epsilon\frac{B}{r^*}. \qquad \text{(A3.1)}$$

Equation A1.3 still holds, and using Eq. A3.1 we obtain

$$r_1 = 4\pi^2\frac{R^2}{r^*\alpha}B. \qquad \text{(A3.2)}$$

Combining Eqs. A1.6 and A3.2 yields

$$\left.\frac{\partial E}{\partial R}\right|_{r(R)} = 4\pi^2\rho_m K_s B.$$

Integration gives the change of energy, ΔE, as the pore migrates from R_i to R_f:

$$\Delta E = 4\pi^2\rho_m K_s B(R_f - R_i). \qquad \text{(A3.3)}$$

We thank Misha Kozlov and Adrian Parsegian for fruitful discussions. We would also like to thank Peter Bronk and Vladik Ratinov for their help with the three-dimensional graphs. Michael J. Curran performed the experiments in Fig. 1 *A* and 9, and Gregory B. Melikyan performed the experiment in Fig. 1 *B*.

We are grateful for the support of the Russian Foundation for Basic Science grant N 93-04-20590 to Y.A.C. and NIH grant GM27367 to F.S.C.

REFERENCES

Breckenridge, L. J., and W. Almers. 1987. Currents through the fusion pore that forms during exocytosis of a secretory vesicle. *Nature.* 328: 814–817.

Chernomordik, L. V., S. I. Sarharv, S. V. Popov, V. P. Pastushemo, A. V. Sokirko, I. G. Abidor, and Y. A. Chizmadzhev. 1987. The electrical breakdown of cell and lipid membranes, the similarity of phenomenologies. *Biochim. Biophys. Acta.* 920:360–373

Chizmadzhev, Y. A., F. S. Cohen, A. Shcherbakov, and J. Zimmerberg. 1995. Theoretical model of fusion pore evolution. *Biol. Membrany.* 12:156–169.

Curran, M. J., F. S. Cohen, D. E. Chandler, P. J. Munson, and J. Zimmerberg. 1993. Exocytotic fusion pores exhibit semi-stable states. *J. Membr. Biol.* 133:61–75.

Deryaguin, B. V., and Yu. V. Gutop. 1962. The theory of the rupture of free films. *Kolloidniy J.* 24:431–437.

Evans, E. A., and R. Skalak. 1980. Mechanics and Thermodynamics of Biomembranes. CRC, Boca Raton, FL. 254.

Hahn, G. H., and S. S. Shapiro. 1967. *Statistical Models in Engineering*, John Wiley & Sons, New York, NY. pp 299.

Helfrich, W. 1973. Elastic properties of lipid bilayers: theory and possible experiments. *Z. Naturforsch.* 28:693–703.

Kozlov, M. M., S. L. Leikin, L. V. Chernomordik, V. S. Markin, and Y. A. Chizmadzhev. 1989. Stalk mechanism of vesicle fusion. Intermixing of aqueous contents. *Eur. Biophys. J.* 17:121–129.

Kozlov, M. M., and V. S. Markin. 1987. Model of red blood cell membrane skeleton: electrical and mechanical properties. *J. Theor. Biol.* 129: 439–452.

Kreyszig, E. 1993. Advanced Engineering Mathematics, 7th ed. John Wiley and Sons, New York.

Kubo, R., M. Toda, and N. Hashitsume. 1991. Statistical Physics II, 2nd ed. Springer-Verlag, Berlin.

Lollike, K., N. Borregaard, and M. Lindau. 1995. The exocytotic fusion pore of small granules has a conductance similar to an ion channel. *J. Cell Biol.* 129:99–104.

Melikyan, G. B., W. D. Niles, and F. S. Cohen. 1993a. Influenza virus hemagglutinin-induced cell-planar bilayer fusion: quantitative dissection of fusion pore kinetics into stages. *J. Gen. Physiol.* 102:1151–1170.

Melikyan, G. B., W. D. Niles, M. E. Peeples, and F. S. Cohen. 1993b. Influenza hemagglutinin-mediated fusion pores connecting cells to planar membranes: flickering to final expansion. *J. Gen. Physiol.* 102: 1131–1149.

Meunier, J., D. Langevin, and N. Boccara. 1987. Physics of Amphiphilic Layers. Springer-Verlag, Berlin.

Monck, J. R., G. A. de Toledo, and J. J. Fernandez. 1990. Tension in secretory granule membranes causes extensive membrane transfer through the exocytotic fusion pore. *Proc. Natl. Acad. Sci. USA.* 87: 7804–7808.

Monck, J. R., A. Oberhauser, G. A. de Toledo, and J. M. Fernandez. 1991. Is swelling of the secretory granule matrix the force that dilates the exocytotic fusion pore? *Biophys. J.* 59:38–47.

Moss, F., and P. V. E. McClintock. 1989. Noise in Nonlinear Dynamical Systems. Vol. 1: Theory of Continuous Fokker-Planck Systems. Cambridge University Press, Cambridge.

Nanavati, C., V. S. Markin, A. F. Oberhauser, and J. M. Fernandez. 1992. The exocytotic fusion pore modeled as a lipidic pore. *Biophys. J.* 63:1118–1132.

Needham, D., and D. A. Haydon. 1983. Tensions and free energies of formation of "solventless" lipid bilayers. *Biophys. J.* 41:251–257.

Plonsky, I., and J. Zimmerberg. 1994. Direct measurement of fusion pore conductance during virus-induced cell-cell fusion. *Biophys. J.* 66:A388.

Siegel, D. P. 1993. Energetics of intermediates in membrane fusion: comparison of stalk and inverted micellar mechanisms. *Biophys. J.* 65:2124–2140.

Spruce, A. E., L. J. Breckenridge, A. K. Lee, and W. Almers. 1990. Properties of the fusion pore that forms during exocytosis of a mast cell secretory vesicle. *Neuron.* 4:643–654.

Spruce, A. E., I. Iwata, and W. Almers. 1991. The first milliseconds of the pore formed by a fusogenic viral envelope protein during membrane fusion. *Proc. Natl. Acad. Sci. USA.* 88:3623–3627.

Spruce, A. E., A. Iwata, J. M. White, and W. Almers. 1989. Patch clamp studies of single cell-fusion events mediated by a viral fusion protein. *Nature.* 342:555–558.

Tse, F. W., A. Iwata, and W. Almers. 1993. Membrane flux through the pore formed by a fusogenic viral envelope protein during cell fusion. *J. Cell Biol.* 121:543–552.

White, J. M. 1992. Membrane fusion. *Science.* 258:917–924.

Zimmerberg, J., R. Blumenthal, D. P. Sarkar, M. Curran, and S. J. Morris. 1994. Restricted movement of lipid and aqueous dyes through pores formed by influenza hemagglutinin during cell fusion. *J. Cell Biol.* 127:1885–1894.

Zimmerberg, J., M. Curran, F. S. Cohen, and M. Brodwick. 1987. Simultaneous electrical and optical measurements show that membrane fusion precedes secretory granule swelling during exocytosis of beige mouse mast cells. *Proc. Natl. Acad. Sci. USA.* 84:1585–1589.

Zimmerberg, J., S. S. Vogel, and L. V. Chernomordik. 1993. Mechanisms of membrane fusion. *Annu. Rev. Biophys. Biomol. Struct.* 22:433–466.